Mitigating Communication Delays in Remotely Connected Hardware-in-the-Loop Experiments

James L. Cale, *Senior Member, IEEE*, Brian B. Johnson, *Member, IEEE*, Emiliano Dall'Anese, *Member, IEEE*, Peter M. Young, *Senior Member, IEEE*, Gerald Duggan, Poorva A. Bedge, *Student Member, IEEE*, Daniel Zimmerle, *Member, IEEE*, and Leah Holton

***Abstract*—This paper introduces a potential approach for mitigating the effects of communication delays between multiple, closed-loop hardware-in-the-loop experiments which are virtually connected, yet physically separated. The approach consists of an analytical procedure for the compensation of communication delays, along with the supporting computational and communication infrastructure. The control design leverages tools for the design of observers for the compensation of measurement errors in systems with time-varying delays. The proposed methodology is validated through computer simulation and hardware experimentation connecting hardware-in-the-loop experiments conducted between laboratories separated by a distance of over 100 km.**

***Index Terms*—Delay compensation, drift observability, hardware-in-the-loop (HIL).**

I. Introduction

SYSTEM emulation using hardware-in-the-loop (HIL) is a frequently used research and validation tool because it enables dynamic cosimulation of models with physical hardware in real time, see [1]–[7]. Several national laboratories, universities, and industrial companies are now pursuing approaches in forming virtually connected simulation testbeds, whereby individual HIL experiments (representing subsystems) at distant locations share state information through communication links to emulate larger, virtually connected systems. Motivation for this research is driven largely by the possibility of sharing experimental resources across large geographical distances without the need for physical relocation of (potentially scarce, sensitive, or massive) research equipment.

Previous research has been performed in connecting geographically separated testbeds in real time, with broad applications. For instance, in [8], a power system for a hybrid electric vehicle using a driver-in-the-loop motion simulator located in Michigan was connected in real time to a hybrid power train in California. To support naval power systems research, the work in [9] used (software-only) simulation of a shipboard power system where components were geographically dispersed and the simulation communicated between laboratories in Mississippi and South Carolina.

To evaluate distributed energy penetration on the U.S. electric grid, a joint experiment analyzing high penetration photovoltaics (PV) on an electrical distribution feeder was performed between two U.S. national laboratories using remote HIL, wherein a large-scale grid simulation (software-only) at a laboratory in Washington was virtually connected with a set of physical, residential PV inverters operating at another laboratory in Colorado [10].

More recently, real-time (software only) simulation of two large ac power systems connected through an HVdc link was performed between laboratories in Norway and Germany [11] and between Germany and South Carolina [12]. Researchers at a national laboratory in Australia performed a closed-loop, remote HIL with a national laboratory in Colorado, where a power network simulator and a physical PV+battery inverter system in the U.S. were virtually connected to a physical PV inverter in Australia to demonstrate coordinated solar PV firming on electrical distribution feeders [13].

However, previous research has not adequately addressed strategies for mitigating communication latencies specific to remotely connected HIL experimentation. As the complexity, number, and physical distances between remotely connected HIL systems increase, it is expected that communication delays will begin to adversely impact the time resolutions possible in multisystem(location) HIL experiments. In particular, communication sampling times between remotely located processors place a fundamental limitation on the effective bandwidth of the combined experiment due to the Nyquist frequency cutoff. Moreover, communication latencies from network traffic and security firewalls at potential host locations can be a significant

Manuscript received February 19, 2017; revised June 25, 2017 and February 1, 2018; accepted March 7, 2018. Date of publication March 30, 2018; date of current version July 30, 2018. This work was supported in part by the National Renewable Energy Laboratory operated for the Department of Energy by the Alliance for Sustainable Energy, LLC under Contract DOE-AC36-08-GO28308. *(Corresponding author: James L. Cale.)*

J. L. Cale, G. Duggan, P. A. Bedge, D. Zimmerle, and L. Holton are with the Department of Mechanical Engineering, Colorado State University, Fort Collins, CO 80523 USA (e-mail: jcale@colostate.edu; jerry.duggan@colostate.edu; poorva.bedge@colostate.edu; dan.zimmerle@colostate.edu; leah.haling@colostate.edu).

B. B. Johnson is with the Department of Electrical Engineering, University of Washington, Seattle, WA 98195 USA (e-mail: brianbj@uw.edu).

E. Dall'Anese is with the National Renewable Energy Laboratory, Golden, CO 80401 USA (e-mail: emiliano.dallanese@nrel.gov).

P. M. Young is with the Department of Electrical Engineering, Colorado State University, Fort Collins, CO 80401 USA (e-mail: peter.young@colostate.edu).

Color versions of one or more of the figures in this paper are available online at http://ieeexplore.ieee.org.

Digital Object Identifier 10.1109/TIE.2018.2821618

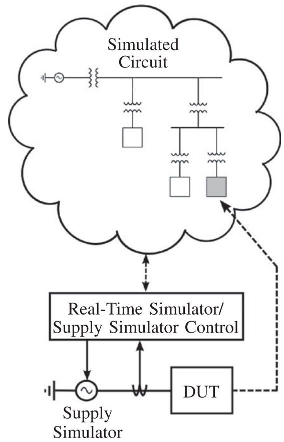

Fig. 1. Configuration for a single HIL experiment.

source of delay. Advanced methods for mitigating communication latencies are needed to enable larger and more complex virtually connected testbeds.

This paper describes a potential control methodology, computational and communications architecture for helping to mitigate the effects of communication delays between remote HIL experiments, and validates the method on an example system through simulation and hardware demonstration.

Key contributions of this paper are: 1) introducing concepts from the control of drift-observable, time-delayed systems as a potential framework and approach for mitigating communication delays in remotely connected HIL systems; and 2) demonstrating the approach in simulation and hardware.

The remainder of this paper is as follows. Section II provides a brief background on HIL and previous research in relevant delay compensation methods, with particular emphasis on observers for time-varying delay systems. This is followed in Section III by a description of the design approach introduced in this paper. The approach is demonstrated on an example system in Section IV. Section V demonstrates a validation of the concept in hardware. This paper concludes with a summary of findings and suggestions for future research in Section VI.

II. Background

A. Brief Overview of HIL Simulation

HIL platforms enable realistic evaluation of physical hardware in the context of a modeled system. Using real-time simulators, models are executed and exchange signals with a physical device under test (DUT) in a closed-loop fashion; an example configuration is depicted in Fig. 1.

In Fig. 1, the supply simulator is a controllable power supply, which is physically connected to the DUT. The real-time simulator computes the response of the simulated circuit (bubbled area in Fig. 1) and provides control signals to the supply simulator. Measurements from the experiment are fed back to the circuit model on the real-time simulator, thus “closing the loop.” In this way, the dynamic response of the DUT inside the model is simulated, i.e., the DUT *appears* to be inside the circuit model (depicted by gray box in Fig. 1).

Single location real-time HIL, including controller HIL and power HIL, have been developed extensively for closed-loop simulations. Examples include the simulation of physical controllers and power devices [1], [2] and for investigating demand-side management techniques for providing grid ancillary services [3]. These simulations have included multiphysics domains as well, e.g., see [4] and [5].

Closed-loop *remote* HIL consists of two or more of the individual HIL systems depicted in Fig. 1, which are physically separated, yet exchange state information through communication links to provide a virtually connected, closed-loop simulation. However, communication latencies between HIL instances are a critical factor in ensuring that the desired bandwidth of the emulated experiment is met. The following sections describe prior research in delay compensation techniques for time-varying delay control systems, which, as will be proposed, provides a basis for a method to mitigate communication latencies in remotely connected HIL systems.

B. Delay Compensation Methods in HIL Simulation

Prior research has been performed on delay compensation for single location HIL simulations. In [14], current filters were incorporated in the feedback path to improve the stability of the closed-loop software $\leftrightarrow$ hardware simulation. Additional approaches to prevent instabilities of the resultant closed-loop system were proposed in [15]. However, the approaches in [14]–[23] focused on single HIL testbeds, and did not address the issue of connecting remote systems through HIL.

The real-time simulation platform developed in [24] was utilized to emulate the operation of cyber-physical energy systems, where control signals for energy resources were dispatched and exchanged through a communication network. The platform combined real-time simulations of dynamic electric models and communication systems, with the goals of assessing the impact of noninstantaneous communications on distributed control tasks and evaluating reconfiguration strategies for the communication systems. Communication protocols were emulated within the HIL platform, but remote communication between HIL instances was not considered.

Communication and processing delays in wide area control systems were evaluated in [25]. Communication delays were estimated from empirical measurements from a transmission system; operational delays were then estimated and assessed via (single location) HIL.

The work in [26] considered remote access to HIL simulators to control a dynamical system. The framework was demonstrated for remote control of a robotic arm. The main objective was to provide control and simulation capabilities without physical existence of the equipment in the laboratory. The framework was close in spirit to the method presented in this paper; however, the work in [26] did not consider utilizing HIL for testing and emulating remote HIL systems or assess the impact of communication delays on the control and emulation tasks.

Focusing on general (non)linear dynamical systems, an approach for the construction of a state observer for nonlinear systems when the output measurements have nonnegligible time delays was proposed in [27]. Algorithms for estimating the system state in the presence of different communication delays were proposed, and conditions ensuring global exponential convergence to zero of the estimation error for any given value of the delay in the measurements were derived. Closely related work in [28]–[30] described the design of observers that are guaranteed to asymptotically converge to the values of the actual (nondelayed) system output.

As described in the following sections, the theory for observer design for systems with time-varying delays described in [27]–[30] provides a potential building block for mitigating the effect of communication delays between remote HIL experiments, as described in this paper. Combined with a cyber-physical architecture for the HIL configuration(s), design, and selective placement of embedded observers, the proposed approach leverages the theory in [27]–[30] to provide a framework for compensating delays between remotely connected HIL simulations to produce a system simulation that appears virtually connected (i.e., colocated).

C. Observers for Time-Varying Delay Systems

This section provides a condensed summary of key research findings on observer design for systems with time-varying delays described in [27]–[30], which will be referred to in subsequent sections.

Notation: Upper-case (lower-case) boldface letters will be used for matrices (column vectors); $(\cdot)^T$ denotes transposition; $|\cdot|$ denotes the absolute value of a number or cardinality of a set; ∇ stands for the gradient operator; $\langle \mathbf{x}, \mathbf{y}\rangle$ denotes the inner product of vectors $\mathbf{x}$ and $\mathbf{y}$. For a given $N \times 1$ vector $\mathbf{x} \in \mathbb{R}^n$, x_i denotes its ith component, and $\|\mathbf{x}\|_2 := \sqrt{\mathbf{x}^T\mathbf{x}}$. $\mathcal{C}^\infty$ denotes the field of infinitely differentiable functions.

Consider the following dynamical system describing the evolution of a state vector $\mathbf{x}(t) \in \mathbb{R}^n$:

$$\dot{\mathbf{x}}(t) = \mathbf{f}\left(\mathbf{x}(t)\right) + \mathbf{g}(\mathbf{x}(t), \mathbf{u}(t)) \tag{1a}$$

$$\bar{y}(t) = h\left(\mathbf{x}(t-\delta(t))\right) \tag{1b}$$

where $\mathbf{u}(t) \in \mathbb{R}^m$ is a known input vector, functions $\mathbf{f} : \mathbb{R}^n \to \mathbb{R}^n$, $\mathbf{g} : \mathbb{R}^n \times \mathbb{R}^m \to \mathbb{R}^n$, and $h : \mathbb{R}^n \to \mathbb{R}$ are in $\mathcal{C}^\infty$, and $\bar{y}(t)$ represents a measurement of the *delayed* state vector $\mathbf{x}$ at time $t - \delta(t)$. Particularly, $\delta(t) \in [0, \Delta]$, $\forall\, t$ represents a known, time-varying and bounded measurement delay. The objective of [27]–[30] is to design an observer to predict $\mathbf{x}(t)$ by processing the delayed measurement $\bar{y}(t)$.

Let $\xi : \mathbb{R}^n \to \mathbb{R}$ be an infinitely differentiable function, and consider a vector field $\mathbf{v} : \mathcal{S} \to \mathbb{R}^n$, $\mathcal{S} \subseteq \mathbb{R}^n$. Suppose that $\mathbf{v}(\mathbf{x}) \in \mathcal{C}^\infty$. The Lie derivative of the function $\xi(\mathbf{x})$ along the vector field $\mathbf{v}$ is defined as follows:

$$L_{\mathbf{v}}\xi(\mathbf{x}) := \langle\, \nabla\xi(\mathbf{x}), \mathbf{v}(\mathbf{x})\,\rangle = \sum_{i=1}^{n} \frac{\partial \xi(\mathbf{x})}{\partial x_i} v_i(\mathbf{x})\,. \tag{2}$$

The kth Lie derivative of $\xi(\mathbf{x})$, denoted $L^k_{\mathbf{v}}\xi(\mathbf{x})$, is obtained by k-times repeated iteration of $L_{\mathbf{v}}\xi(x)$ and $L^0_{\mathbf{v}}\xi(\mathbf{x}) := \xi(\mathbf{x})$.

Consider the following mapping associated with functions $\mathbf{f}(\cdot)$ and $h(\cdot)$ in (1):

$$\mathbf{\Phi}(\mathbf{x}) := \begin{bmatrix} h(\mathbf{x}) & L_{\mathbf{f}}h(\mathbf{x}) & \cdots & L^{n-1}_{\mathbf{f}}h(\mathbf{x}) \end{bmatrix}^T. \tag{3}$$

System (1) is said to be *globally drift-observable* if $\mathbf{\Phi}(\mathbf{x})$ is a diffeomorphism on $\mathbb{R}^n$. Drift-observability of (1) implies that the Jacobian $\mathbf{J}(\mathbf{x})$ associated with $\mathbf{\Phi}(\mathbf{x})$ is nonsingular for all $\mathbf{x} \in \mathbb{R}^n$, in which case the mapping $\mathbf{z} = \mathbf{\Phi}(\mathbf{x})$ defines a global change of coordinates.

Suppose that system (1) is globally drift-observable, and has the following additional properties: *(P1)* The triple $(\mathbf{f}, \mathbf{g}, h)$ has *uniform observation degree* at least equal to n defined as follows:

$$L_{\mathbf{g}}L^k_{\mathbf{f}}h(\mathbf{x}) = 0, \quad k = 0, \ldots, n-2,\ \forall \mathbf{x} \in \mathbb{R}^n \tag{4}$$

$$L_{\mathbf{g}}L^{n-1}_{\mathbf{f}}h(\mathbf{x}) \neq 0, \quad \text{for some } \mathbf{x} \in \mathbb{R}^n \tag{5}$$

in which case, the following function is well-defined

$$p(\mathbf{z}, \mathbf{u}) = \left(L^n_{\mathbf{f}}h(\mathbf{x}) + L_{\mathbf{g}}L^{n-1}_{\mathbf{f}}h(\mathbf{x})\mathbf{u}\right)_{\mathbf{x}=\mathbf{\Phi}^{-1}(\mathbf{z})}. \tag{6}$$

(P2) Function $p(\mathbf{z}, \mathbf{u})$ in (6) is globally uniformly Lipschitz continuous with respect to $\mathbf{z}$, and the Lipschitz coefficient $\gamma(\|\mathbf{u}\|)$ is a nondecreasing function of $\|\mathbf{u}\|$; i.e., for any $\mathbf{z}_1, \mathbf{z}_2 \in \mathbb{R}^n$, it holds that

$$\|p(\mathbf{z}_1, \mathbf{u}) - p(\mathbf{z}_2, \mathbf{u})\| \leq \gamma(\|\mathbf{u}\|)\|\mathbf{z}_1 - \mathbf{z}_2\|\,. \tag{7}$$

If (1) is globally uniformly Lipschitz drift-observable (GULDO) with properties (P1) and (P2), then the following observer associated with system (1) can be constructed

$$\dot{\hat{\mathbf{x}}}(t) = \mathbf{f}\left(\hat{\mathbf{x}}(t)\right) + \mathbf{g}\left(\hat{\mathbf{x}}(t)\mathbf{u}(t)\right) + \mathbf{J}^{-1}(\hat{\mathbf{x}}(t))\mathbf{k}_\delta\left[\bar{y}(t) - h\left(\hat{\mathbf{x}}(t-\delta(t))\right)\right],\quad t \geq 0 \tag{8a}$$

$$\mathbf{k}_\delta = e^{-\rho\delta}\mathbf{k}_0 \tag{8b}$$

where vector $\mathbf{k}_0 \in \mathbb{R}^n$ and scalar $\rho \geq 0$ are design parameters. Theorem 1 in [28] asserts that if input $\|\mathbf{u}(t)\| \leq u_M$ for some constant u_M, then for a decay rate $\rho \geq 0$ and bounded delay $\delta(t) \in [0, \Delta]$ there exists a vector $\mathbf{k}_0 \in \mathbb{R}^n$ such that

$$\|\mathbf{x}(t) - \hat{\mathbf{x}}(t)\| \leq ce^{-\rho t}, \quad t \geq 0 \tag{9}$$

for some constant c, i.e, $\hat{\mathbf{x}}(t)$ asymptotically converges to the ideal (nondelayed) system state $\mathbf{x}(t)$. Furthermore, the theorem states that if vector $\mathbf{k}_0$ satisfies the matrix inequality

$$(\mathbf{A}_n - \mathbf{k}_0\mathbf{C}_n)^T\mathbf{P} + \mathbf{P}(\mathbf{A}_n - \mathbf{k}_0\mathbf{C}_n) + (2\rho + \beta + \kappa)\mathbf{P} + \gamma^2_M(\mathbf{B}^T_n\mathbf{P}\mathbf{B}_n)\mathbf{I}_{n\times n} \leq \mathbf{0} \tag{10}$$

where $(\mathbf{A}_n, \mathbf{B}_n, \mathbf{C}_n)$ are a Brunowski triple of order n, γ_M is the Lipschitz coefficient associated with u_M, $\beta > 0$ and $\kappa > 1$ design parameters, and $\mathbf{P}$ is symmetric positive definite, then exponential-decay state tracking [cf., (9)] is guaranteed for

$$\Delta \leq \bar{\Delta} := \frac{\beta}{2 + (\mathbf{k}^T_0\mathbf{P}\mathbf{k}_0)\|\mathbf{P}^{-1}\|(1 + \rho^2 + \mathbf{C}^2_n\mathbf{k}^2_1)\kappa}\,. \tag{11}$$

Remark: it is important to note that the theory derived in [27]–[30] and summarized in (1)–(11) assumes control of a single system. While we use the structure of the observer design

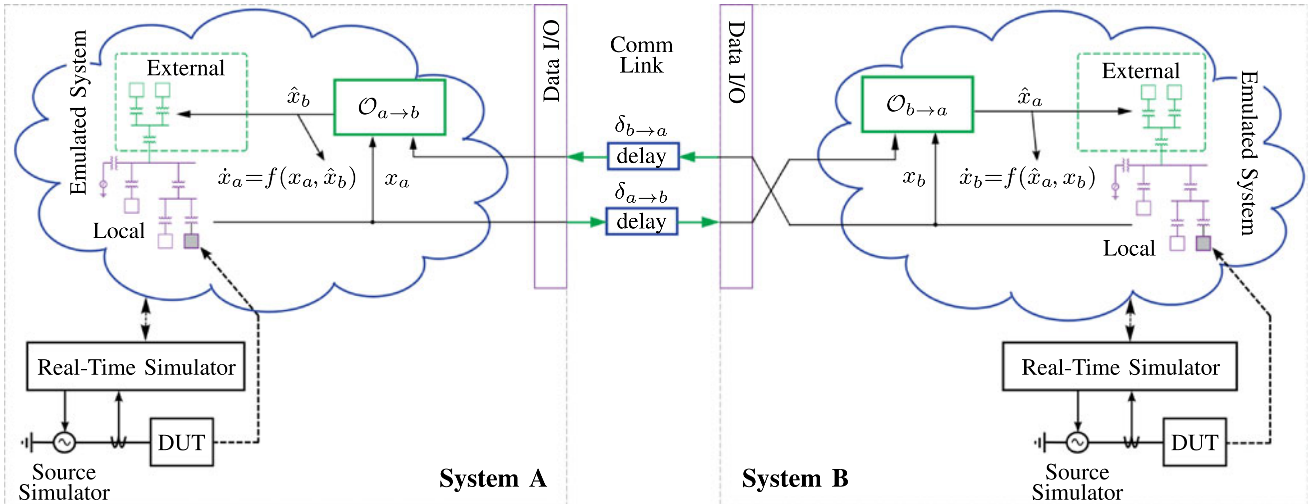

Fig. 2. Conceptual model of ODC architecture for two HIL systems connected via a communication link.

in (8) as a guide for the design of observers for remote HIL applications (with justification explained in the next section), convergence for multiple HIL systems must be verified in simulation until the convergence guarantee in (11) is extended and rigorously proven for multiple HIL instances; this an objective of future research.

III. Embedded Observers for Remote HIL Applications

This section explains how the theory in the previous section can be adapted to help mitigate communication delays in remote HIL applications, hereafter referred to as the observer delay compensation (ODC) approach. The central concept is depicted in Fig. 2. As shown in Fig. 2, the mathematical description of System A(B) is a function of both locally obtained (measured or computed) state information $x_{a(b)}$ and estimates of remote states $\hat{x}_{b(a)}$. Estimates for remote states occurring at System A(B) are computed in *observers* located at System B(A). In control theory, observers are commonly used to estimate actual state variables based on known information, such as measurements [31]. The notation $\mathcal{O}_{x\to y}$ denotes an observer at System X that estimates delayed states received from System Y; $\delta_{x\to y}$ denotes the communication delay between System X and System Y.

In Fig. 2, delayed measurements from the remote system(s) along with knowledge of its mathematical representation are used to provide an estimate of the nondelayed remote states, through the use of embedded observers. Errors in the predicted states are then dynamically corrected as new information is obtained from the remote system(s). For simplicity, we assume herein that locally measured signals do not contain delay; only communication between remote systems is considered.

Lacking a formal convergence guarantee for multiple HIL instances corresponding to [27]–[30] at the time of the experimental work, the observer designs were performed *quasi-heuristically* with (1)–(8) as a guide. In particular, we assumed that if: 1) Systems A and B in Fig. 2 could both be shown to be GULDO and possess properties (P1) and (P2); 2) observers for the system were constructed using (8) (which is always possible if the first condition is satisfied); and 3) the upper bound on the communication delay between the two systems could be estimated with reasonable certainty. Then, design parameter $\mathbf{k}_0$ in (8) *may* exist such that all states in the complete system converged asymptotically, which we could validate through computer simulation before hardware implementation.

The assumptions above were based on the following reasoning. When designing observers to estimate the state vectors $\mathbf{x} \in \mathbb{R}^N$, $N \leq n$ at each location for an n-dimensional total system, drift-observability of each subsystem ensures the Jacobian $\mathbf{J}(\mathbf{x})$ in (8) is nonsingular for all $\mathbf{x} \in \mathbb{R}^N$, the guarantee of observation degree $\geq n$ ensures the subsystems are observable, and global uniform Lipschitz continuity ensures adjustment (i.e., feedback control) of states occurs along smooth and well-defined trajectories.

Guided by this reasoning, the design approach for constructing embedded observers to implement the ODC method consists of the following steps.

1) Derivation of the mathematical description of the virtually connected subsystems.
2) Check of GULDO and properties (P1) and (P2) for each subsystem.
3) Construction of observers using (8) and selection of $\mathbf{k}_0$ for each location.
4) Validation of system convergence (e.g., in simulation).

What follows is a demonstration of the above steps on an example system partitioned into two subsystems.

IV. Design Example

A. Mathematical Description

Consider the electrical circuit shown in Fig. 3 containing two current sources $i_{1(2)}$ in parallel with shunt capacitors $C_{1(2)}$, and connected through a series RL impedance.

The equation describing each of the $k \in \{1, 2\}$ sources is

$$\frac{di_k}{dt} = \eta_k \left(v_k - e_k^*\right) + \alpha_k i_k \tag{12}$$

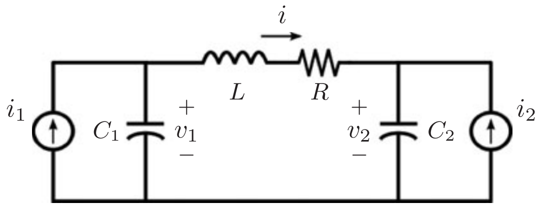

Fig. 3. Example electrical circuit (ideal).

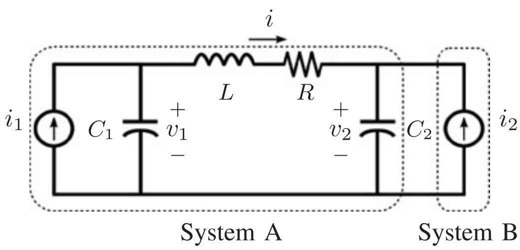

Fig. 4. Partitioned system (partition boundaries shown as dashed lines).

where it is assumed that the sources represent *composite* current supplies which include externally connected voltage sources downstream; this is used to introduce transient inputs to the simulation. Here, e_k^* represents connected (and potentially time-varying) voltage input signals, η_k are voltage error gains, and $\alpha_k < 0$ are damping factors.

This system can be represented in state-space form

$$\frac{d\mathbf{x}}{dt} = \mathbf{A}\mathbf{x} + \mathbf{B}\mathbf{u} \tag{13}$$

where the vector of states $\mathbf{x} = \begin{bmatrix} i_1 & i_2 & v_1 & v_2 & i \end{bmatrix}^T$

$$\mathbf{A} = \begin{bmatrix} \alpha_1 & 0 & \eta_1 & 0 & 0 \\ 0 & \alpha_2 & 0 & \eta_2 & 0 \\ 1/C_1 & 0 & 0 & 0 & -1/C_1 \\ 0 & 1/C_2 & 0 & 0 & 1/C_2 \\ 0 & 0 & 1/L & -1/L & -R/L \end{bmatrix}, \mathbf{B} = \begin{bmatrix} -\eta_1 & 0 \\ 0 & -\eta_2 \\ 0 & 0 \\ 0 & 0 \end{bmatrix} \tag{14}$$

and the input vector $\mathbf{u} = [e_1^* \; e_2^*]^T$.

Suppose we wish to partition the system in Fig. 3 so portions can be simulated remotely, yet remain coupled through mutual exchange of state information. First, consider a partitioning of the system into two (sub)systems, referred to herein as "System A" and "System B," as shown in Fig. 4.

Next, consider the physical separation and control of Systems A and B where each is controlled in the following manner. First, replace System B in Fig. 4 with a controllable current source that injects estimated input current $\hat{i}_2$ into System A, as shown in the left of Fig. 5. Then, replace System A in Fig. 4 with a controllable voltage source that provides estimated voltage $\hat{v}_2$ to System B as shown on right of Fig. 5.

System A in Fig. 5 can be described in state-space as

$$\frac{d\mathbf{x}_a}{dt} = \mathbf{A}_a\mathbf{x}_a + \mathbf{B}_a\mathbf{u}_a \tag{15}$$

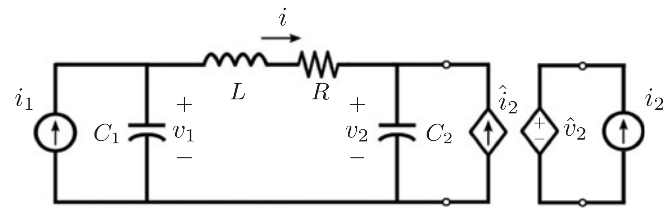

Fig. 5. Systems A and B with remote inputs $\hat{i}_2$ and $\hat{v}_2$, respectively.

where the vector of states $\mathbf{x}_a = [i_1 \; v_1 \; i \; v_2]^T$

$$\mathbf{A}_a = \begin{bmatrix} \alpha_1 & \eta_1 & 0 & 0 \\ 1/C_1 & 0 & -1/C_1 & 0 \\ 0 & 1/L & -R/L & -1/L \\ 0 & 0 & 1/C_2 & 0 \end{bmatrix}, \mathbf{B}_a = \begin{bmatrix} -\eta_1 & 0 \\ 0 & 0 \\ 0 & 0 \\ 0 & 1/C_2 \end{bmatrix} \tag{16}$$

and the input vector $\mathbf{u}_a = \begin{bmatrix} e_1^* & \hat{i}_2 \end{bmatrix}^T$. The nominal output of System A *at System A* is $v_2(t)$, the delayed output $\bar{y}_a(t) = v_2(t - \delta(t))$ in (1), is obtained by defining matrix $\mathbf{C}_a$ as

$$\begin{aligned} \bar{\mathbf{y}}_a(t) &= \mathbf{C}_a\mathbf{x}_a(t - \delta(t)) \\ &= \begin{bmatrix} 0 \; 0 \; 0 \; 1 \end{bmatrix} \mathbf{x}_a(t - \delta(t)) \\ &= v_2(t - \delta(t)). \end{aligned} \tag{17}$$

For System B, the state-space representation is

$$\frac{d\mathbf{x}_b}{dt} = \mathbf{A}_b\mathbf{x}_b + \mathbf{B}_b\mathbf{u}_b \tag{18}$$

where the state vector $\mathbf{x}_b = [\, i_2 \,]$

$$\mathbf{A}_b = \begin{bmatrix} \alpha_2 \end{bmatrix}, \; \mathbf{B}_b = \begin{bmatrix} -\eta_2 & \eta_2 \end{bmatrix} \tag{19}$$

and the input vector $\mathbf{u}_b = \begin{bmatrix} e_2^* & \hat{v}_2 \end{bmatrix}^T$ The nominal output of System B *at System B* is $i_2(t)$, so matrix $\mathbf{C}_b$ is defined as

$$\begin{aligned} \bar{\mathbf{y}}_b(t) &= \mathbf{C}_b\mathbf{x}_b(t - \delta(t)) \\ &= [1][i_2(t - \delta(t))] \\ &= i_2(t - \delta(t)). \end{aligned} \tag{20}$$

For System A note from comparison of (1) and (15)–(17)

$$\mathbf{f}(\mathbf{x}(t)) \mapsto \mathbf{A}_a\mathbf{x}_a(t) \tag{21}$$

$$\mathbf{g}(\mathbf{x}(t))\mathbf{u}(t) \mapsto \begin{bmatrix} -\eta_1 e_1^*(t) & 0 & 0 & 0 \end{bmatrix}^T \tag{22}$$

$$\mathbf{h}(\mathbf{x}(t - \delta(t))) \mapsto \mathbf{C}_a\mathbf{x}_a(t - \delta(t)) = v_2(t - \delta(t)). \tag{23}$$

The mapping $\mathbf{z}_b = \mathbf{\Phi}(\mathbf{x}_a)$ for System A, with $n = 4$ is

$$\mathbf{\Phi}(\mathbf{x}_a) = \begin{bmatrix} 0 & 0 & 0 & 1 \\ 0 & 0 & 1/C_2 & 0 \\ 0 & 1/LC_2 & -R/LC_2 & -1/LC_2 \\ \sigma_1 & \sigma_2 & \sigma_3 & \sigma_4 \end{bmatrix} \mathbf{x}_a = \mathbf{\Lambda}_a\mathbf{x}_a \tag{24}$$

where $\sigma_1 = 1/LC_1C_2$, $\sigma_2 = -1/LC_1C_2 - R/L^2C_2$, $\sigma_3 = -R^2/L^2C_2 - 1/LC_2^2$, and $\sigma_4 = R/L^2C_2$. Note that the mapping $\mathbf{\Phi}(\mathbf{x}_a)$ is diffeomorphic if $\mathbf{\Lambda}_a$ defined in (24) is invertible, which is determined by the values of the circuit parameters. From (24)

$$\mathbf{J}_a(\mathbf{x}_a) = \begin{bmatrix} 0 & 0 & 0 & 1 \\ 0 & 0 & 1/C_2 & 0 \\ 0 & 1/LC_2 & -R/LC_2 & -1/LC_2 \\ \sigma_1 & \sigma_2 & \sigma_3 & \sigma_4 \end{bmatrix} = \mathbf{\Lambda}_a \tag{25}$$

which is indeed nonzero for all $\mathbf{x}_a \in \mathbb{R}^4$. For property (P1), it is easy to verify that $L_\mathbf{g} L_\mathbf{f}^k \mathbf{h}(\mathbf{x}) = 0$ for $k = 0, \ldots, n-2$, $\forall \mathbf{x} \in \mathbb{R}^n$. The second condition in (P1) holds since $L_\mathbf{g} L_\mathbf{f}^3 \mathbf{h}(\mathbf{x}_a) = \mathbf{\Gamma}\mathbf{g}(\mathbf{x}(t))\mathbf{u}(t)$ where $\mathbf{\Gamma} := [\varsigma_1\ \varsigma_2\ \varsigma_3\ \varsigma_4]$, $\varsigma_1 = 1/LC_1C_2$, $\varsigma_2 = -R/L^2C_2$, $\varsigma_3 = (-1/LC_1C_2 + R^2/L^2C_2 - 1/L^2C_2)$, $\varsigma_4 = R/L^2C_2$. Therefore, $L_\mathbf{g} L_\mathbf{f}^3 \mathbf{h}(\mathbf{x}_a) = -\eta_1 \varsigma_1 e_1^*(t) \neq 0$ for some $\mathbf{x}_a \in \mathbb{R}^4$, in particular whenever the signal $e_1^*(t) \neq 0$. As expected, $p(\mathbf{z}_a, \mathbf{u}_a)$ is well-defined

$$\begin{aligned} p(\mathbf{z}_a, \mathbf{u}_a) &= \left(L_\mathbf{f}^4 \mathbf{h}(\mathbf{x}_a) + L_\mathbf{g} L_\mathbf{f}^3 \mathbf{h}(\mathbf{x}_a)\mathbf{u}_a\right)_{\mathbf{x}_a = \mathbf{\Phi}^{-1}(\mathbf{z}_a)} \\ &= \mathbf{\Gamma}\mathbf{x}_a - \eta_1 \varsigma_1 (e_1^*(t))^2 \\ &= \mathbf{\Gamma}\mathbf{\Lambda}_a^{-1}\mathbf{z}_a - \eta_1 \varsigma_1 (e_1^*(t))^2. \end{aligned} \tag{26}$$

Considering property (P2) for System A, note that $p(\mathbf{z}_a, \mathbf{u}_a)$ is globally uniformly Lipschitz continuous with respect to $\mathbf{z}_a$; its derivative with respect to this variable is equal to (constant) $\mathbf{\Gamma}\mathbf{\Lambda}_a^{-1}$. The Lipschitz coefficient can be determined from (7) to derive the requirement that $\gamma \geq \|\mathbf{\Gamma}\mathbf{\Lambda}_a^{-1}\|$ and is therefore nondecreasing in $\|\mathbf{u}_a\|$.

For System B, note from comparison of (1) and (18) and (20),

$$\mathbf{f}(\mathbf{x}(t)) \mapsto \mathbf{A}_b \mathbf{x}_b(t) = \alpha_2 i_2(t) \tag{27}$$

$$\mathbf{g}(\mathbf{x}(t))\mathbf{u}(t) \mapsto -\eta_2 e_2^*(t) \tag{28}$$

$$\mathbf{h}(\mathbf{x}(t - \delta(t))) \mapsto \mathbf{C}_b \mathbf{x}_b(t - \delta(t)) = i_2(t - \delta(t)). \tag{29}$$

The mapping $\mathbf{z}_b = \mathbf{\Phi}(\mathbf{x}_b)$ for System B with $n = 1$ is

$$\mathbf{\Phi}(\mathbf{x}_b) = \mathbf{x}_b = i_2(t). \tag{30}$$

Functions of the form $\Phi(x) = x$, $x \in \mathbb{R}$ are diffeomorphic and $\mathbf{\Phi}(\mathbf{x}_b)$ is a diffeomorphism for $\mathbf{x}_b \in \mathbb{R}$. The Jacobian for System B

$$\mathbf{J}_b(\mathbf{x}_b) = 1 \tag{31}$$

which is indeed nonzero for all $\mathbf{x}_b \in \mathbb{R}$.

We now examine whether System B possesses properties (P1) and (P2). For the first property, note that the first condition in (6) doesn't apply since $n = 1$. The second condition is true since $L_\mathbf{g} L_\mathbf{f}^0 \mathbf{h}(\mathbf{x}_b) = -\eta_2 e_2^*(t) \neq 0$, for some $\mathbf{x}_b \in \mathbb{R}$, in particular whenever $e_2^*(t) \neq 0$. Note the function

$$\begin{aligned} p(\mathbf{z}_b, \mathbf{u}_b) &= \left(L_\mathbf{f}^n \mathbf{h}(\mathbf{x}_b) + L_\mathbf{g} L_\mathbf{f}^{n-1} \mathbf{h}(\mathbf{x}_b)\mathbf{u}_b\right)_{\mathbf{x}_b = \mathbf{\Phi}^{-1}(\mathbf{z}_b)} \\ &= \alpha_2 \mathbf{z}_b - \eta_2 (e_2^*(t))^2 \end{aligned} \tag{32}$$

is indeed well-defined. Considering property (P2) for System B, note that $p(\mathbf{z}_b, \mathbf{u}_b)$ is globally uniformly Lipschitz continuous with respect to $\mathbf{z}_b$; its derivative with respect to $\mathbf{z}_b$ is equal to constant α_2 for all $\mathbf{z}_b \in \mathbb{R}$. The Lipschitz coefficient can be determined from the inequality

$$\begin{aligned} \|p(\mathbf{z}_{b,1}, \mathbf{u}_b) - p(\mathbf{z}_{b,2}, \mathbf{u}_b)\| &= \|\alpha_2\|\|\mathbf{z}_{b,1} - \mathbf{z}_{b,2}\| \\ &\leq \gamma(\|\mathbf{u}_b\|)\|\mathbf{z}_{b,1} - \mathbf{z}_{b,2}\| \end{aligned} \tag{33}$$

from which we derive that $\gamma \geq \|\alpha_2\|$, and is therefore nondecreasing in $\|\mathbf{u}_b\|$.

B. Observer Construction and Parameter Selection

The observer $\mathcal{O}_{a\to b}$ estimates input current $\hat{i}_2$ at System A based on measurements of signal $i_2(t - \delta_{b\to a}(t))$ received from System B and is constructed as

$$\begin{aligned} \frac{d\hat{i}_2(t)}{dt} &= \mathbf{A}_b \hat{i}_2(t) + \mathbf{B}_b \mathbf{u}_b + \mathbf{J}_b^{-1}(\hat{i}_2(t))\, \mathbf{k}_{0b} e^{-\rho\delta_{b\to a}} \\ &\quad \left(i_2(t - \delta_{b\to a}(t)) - \hat{i}_2(t - \delta_{b\to a}(t))\right). \end{aligned} \tag{34}$$

The observer $\mathcal{O}_{b\to a}$ estimates voltage $\hat{v}_2(t)$ based on measurements of signal $v_2(t - \delta_{b\to a}(t))$ received from System A and is constructed as

$$\begin{aligned} \frac{d\hat{\mathbf{x}}_a}{dt} &= \mathbf{A}_a \hat{x}_a(t) + \mathbf{B}_a \mathbf{u}_a + \mathbf{J}_a^{-1}(\hat{x}_a(t))\, \mathbf{k}_{0a} e^{-\rho\delta_{a\to b}} \\ &\quad (v_2(t - \delta_{a\to b}(t)) - \hat{v}_2(t - \delta_{a\to b}(t))) \end{aligned} \tag{35}$$

where $\hat{\mathbf{x}}_a = \left[\hat{i}_1\ \hat{v}_1\ \hat{i}\ \hat{v}_2\right]^T$. In (35) and (36), $\mathbf{k}_{0a(b)}$ denotes the parameter $\mathbf{k}_0$ in (8) for the observer that estimates states physically located at System A(B).

A reasonable guess for selecting suitable $\mathbf{k}_{0a(b)}$ (which must be validated, as shown in the next subsection) is to compute the feedback vector for the so-called Luenberger observer [32] corresponding to each of the subsystems. This is the method that was used in this work, where the MathWorks `place` command was used to place closed-loop poles at desired locations to yield satisfactory total system response. Note that it is always possible to obtain these feedback vectors since the subsystems are confirmed to be observable in step B) of the design process.

C. Validation in Simulation

The delay compensation technique was applied to the partitioned circuit in Fig. 4 using the parameter values shown in Table I. [Note that these parameters are not intended to represent a specific system—they were chosen only to clearly visualize the difference in the compensated and uncompensated responses.] The simulations were performed in MathWorks SimPowerSystems toolbox, version 5.7 [33].

The passive circuit elements, error gains and damping factors in Table I were chosen arbitrarily, except that $\mathbf{\Lambda}_a$ in (25) was validated to be invertible. The communication delay T_d was chosen to be several times greater than the empirically measured network delay (approximately 30 ms per round trip, as described in Section V). The update rate τ_u was chosen to be an order of magnitude greater than T_d; the desired convergence rate ρ was arbitrarily chosen to visually observe the response. The vector $\mathbf{k}_{0a}$ was calculated as $[\,4.06\ \ 6.18\ \ 4.18\ \ 1.06\,]^T$ for poles placed at $[\,-1.00\ \ -1.01\ \ -1.02\ \ -1.03\,]^T$. Similarly, $\mathbf{k}_{0b}$ was calculated as $[\,1.0\,]$ for a pole placed at $[\,-1.0\,]$. The selection of

TABLE I
SIMULATION PARAMETERS

Parameter	Value
Capacitances, C_1, C_2	1.0 [F]
Resistance, R	0.5 [Ω]
Inductance, L	1.0 [H]
Voltage Error Gain, η_1	-1.0 [sΩ]$^{-1}$
Voltage Error Gain, η_2	-1.0 [sΩ]$^{-1}$
Damping Factor, α_1	-1.0 [s]$^{-1}$
Damping Factor, α_2	-1.0 [s]$^{-1}$
Communication Delay, T_d	0.20 [s]
External Command Update Rate, τ_u	2.0 [s]
Observer Convergence Rate, ρ	4.0 [ms]

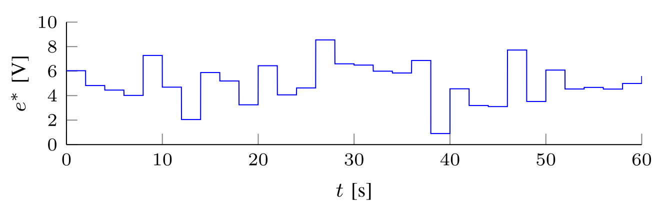

Fig. 6. Signal representing external sources.

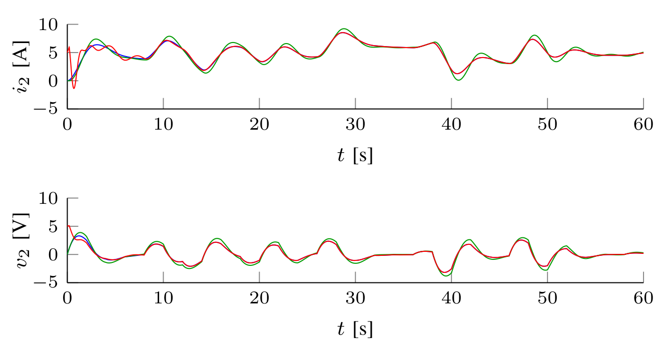

Fig. 7. Simulation results from example partitioned system. Blue lines signify the ideal response (from the ideal circuit in Fig. 3), green lines the uncompensated response, and red lines the observer output.

poles was chosen only to ensure that the full system simulation would be stable and the dynamics would be visible for the choice of system parameters; exploration of system stability with various system and observer parameters choices is a topic of future research.

For simplicity, the input signals $e_1^*(t)$ and $e_2^*(t)$ representing externally connected sources in (12) were both set equal to the waveform $e^*(t)$ depicted in Fig. 6. This function held a (randomly sampled) constant value which was updated every time interval τ_u after the start of the simulation.

The resulting simulation waveforms are shown in Fig. 7. In Fig. 7, the blue lines signify the ideal response (from the ideal circuit in Fig. 3), green lines the uncompensated response, and red lines the observer output. As can be seen, the ideal and observer based ("compensated") signals converge for both voltage and current, despite continued changes in the input signals $e_1^*(t) = e_2^*(t) = e^*(t)$ throughout the simulation.

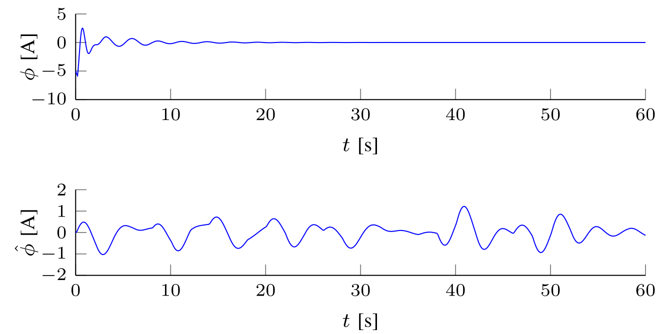

Fig. 8. Errors in i_2 with (upper) and without (lower) delay compensation.

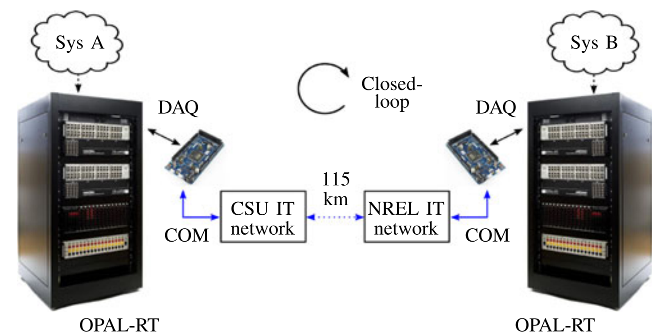

Fig. 9. Hardware in remote Sys A $\leftrightarrows$ Sys B HIL demonstration.

Errors between compensated and uncompensated responses are plotted in Fig. 8 (for current i_2). In particular, $\phi(t)$ is defined as the difference between the compensated and ideal response (blue and red lines in Fig. 7, upper); $\hat{\phi}(t)$ is the difference between the uncompensated and ideal response (green and red lines in Fig. 7, upper).

As shown in Fig. 8, the error in the compensated current signal decreases exponentially to zero, as predicted by (9). Remarkably, once the controller error converges to zero it stays at zero even after the external inputs $e_1^*(t)$, $e_2^*(t)$ continue to change. Note that continued convergence to zero in the compensated systems, despite changing external input signals, are likely possible in this example because models for the full and partitioned systems were known exactly.

V. HARDWARE RESULTS

This section describes experimental validation of the ODC method in hardware. During this experiment, a closed-loop, remote HIL experiment emulating the system shown in Fig. 5, employing the architecture shown in Fig. 2, was performed. This experiment provided a virtual connection of equipment physically located at Colorado State University (CSU), Fort Collins, CO, USA, with equipment located remotely at the National Renewable Energy Laboratory (NREL), Golden, CO, USA. The physical separation between these locations was approximately 115 km. A depiction of the overall experiment is shown in Fig. 9.

In Fig. 9, the System A ("Sys A") and System B ("Sys B") portions of the electrical circuit in Fig. 4 were simulated on OPAL-RT real-time digital simulators [34] at CSU and NREL,

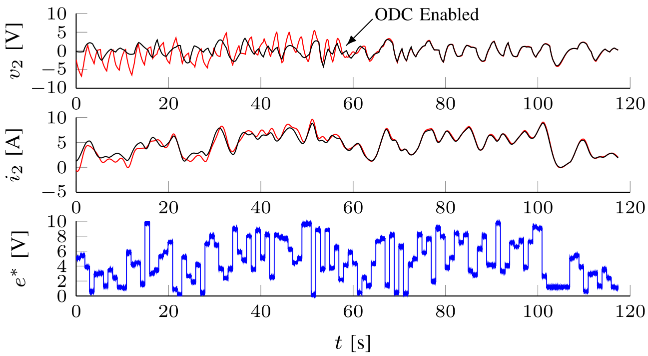

Fig. 10. Measurements from hardware validation of ODC method: compensated signals (red); ideal signals (black); and external input signals (blue).

respectively. The observers for both systems were executed on Arduino EtherDUE [35] at each location. The EtherDUE microcontrollers had a built-in Ethernet port in addition to analog and digital I/O channels.

The observer calculations were executed on the microcontroller boards rather than on the real-time simulators in order to isolate the electrical simulations from the observer computations. This approach provided the following advantages:

1) software for network packet manipulation and time functions were accessible through standard libraries readily installed on the microcontroller boards;
2) processing network signals externally to the real-time simulators eliminated the need for using limited memory and computational resources on the real-time simulators;
3) isolation of the electrical simulation and observers made the architecture more maintainable, since components of the system could be modified and tested independently.

Measurements and observer values were passed between colocated OPAL-RT and Arduino microcontrollers using digital and analog I/O channels. State information was passed between remote locations through the EtherDUE boards using TCP/IP communication. Synchronization between systems was implemented using algorithms on the Arduino boards in a master/slave, hand-shaking configuration.

As mentioned in Section IV, selection of observer parameters and stability analysis for this experiment required an estimate of the network delay between Systems A and B. Since network delays between two systems are generally dependent on many factors (e.g., network load and routing algorithms), the estimated delay was determined experimentally using repeated ping algorithms on the microcontrollers. The sample mean of the round-trip communication delay was found to be $\approx$30 ms.

Measurements obtained during the experiment are shown in Fig. 10. The compensation algorithms were activated at each location at approximately $t = 57$ s. The measurements show that the compensated currents and voltages (red lines) converged to the ideal response signals (black lines) with little error after the delay compensation algorithms converged. Note that as predicted in simulation, once the observer-based delay compensators converged, the error remained near zero even when the external input signal continued to change.

VI. Conclusion and Future Research

This paper introduced a potential method and architecture for helping to mitigate communication delays between remotely connected HIL experiments. Motivation for this paper was the desire to connect geographically distant software/hardware testbeds while minimizing the loss of experimental fidelity arising from communication latencies. The approach was validated through computer simulation and a remote HIL experiment where the subsystems were separated by a physical distance of 115 km and communication delay of 30 ms. However, we note that the convergence results shown in this paper assumed perfect knowledge of the underlying system models. Primary challenges in implementing the method are generating sufficiently accurate mathematical descriptions of the subsystems and determining controller parameters. Automated state-model generation or average value models can possibly be used for more complex systems to address the first challenge. Theoretical development to extend the convergence guarantee for drift-observable, time-delayed observer design for multiple remote systems and design guidelines for optimal parameter selection are needed to resolve the second challenge. Additional future research topics include the addition of robust control techniques to account for potential parameter variations and imperfect system knowledge.

References

[1] M. O. Faruque *et al.*, "Real-time simulation technologies for power systems design, testing, and analysis," *IEEE Power Energy Technol. Syst. J.*, vol. 2, no. 2, pp. 63–73, Jun. 2015.

[2] G. F. Lauss, M. Faruque, K. Schoder, C. Dufour, A. Viehweider, and J. Langston, "Characteristics and design of power hardware-in-the-loop simulations for electrical power systems," *IEEE Trans. Ind. Electron.*, vol. 63, no. 1, pp. 406–417, Jan. 2016.

[3] M. H. Syed, P. Crolla, G. Burt, and J. Kok, "Ancillary service provision by demand side management: A real-time power hardware-in-the-loop co-simulation demonstration," in *Proc. 2015 Int. Symp. Smart Elect. Distrib. Syst. Technol.*, Vienna, Austria, 2015, pp. 492–498.

[4] B. Lu, X. Wu, H. Figueroa, and A. Monti, "A low-cost real-time hardware-in-the-loop testing approach of power electronics controls," *IEEE Trans. Ind. Electron.*, vol. 54, no. 2, pp. 919–931, Mar. 2007.

[5] A. Benigni and A. Monti, "A parallel approach to real-time simulation of power electronics systems," *IEEE Trans. Ind. Electron.*, vol. 30, no. 9, pp. 5192–5206, Sep. 2015.

[6] B. Lundstrom and S. Chakraborty, "An advanced platform for development and evaluation of photovoltaic inverters using hardware-in-the-loop," *Int. J. Distrib. Energy Resources Smart Grids*, vol. 9, no. 1, Mar. 2013.

[7] B. Lundstrom, B. Mather, M. Shirazi, and M. Coddington, "Implementation and validation of advanced unintentional islanding testing using power hardware-in-the-loop (PHIL) simulation," in *Proc. 2013 IEEE 39th Photovoltaic Spec. Conf.*, Tampa Bay, FL, USA, Jun. 2013, pp. 3141–3146.

[8] M. Compere, J. Goodell, M. Simon, W. Smith, and M. Brudnak, "Robust control techniques enabling duty cycle experiments utilizing a 6-DOF crewstation motion base, a full scale combat hybrid electric power system, and long distance internet communications," SAE International, Pittsburgh, PA, USA, Tech. Rep. 2006-01-3077, Nov. 2006.

[9] J. L. Bastos, J. Wu, N. Schulz, R. Liu, and A. Monti, "Distributed simulation using the virtual test bed and its real-time extension," in *Proc. Summer Comput. Simul. Conf.,* San Diego, CA, USA, Jan. 2007, vol. 2, pp. 757–765.

[10] B. Palmintier, B. Lundstrom, S. Chakraborty, T. Williams, K. Schneider, and D. Chassin, "A power hardware-in-the-loop platform with remote distribution circuit cosimulation," *IEEE Trans. Ind. Electron.*, vol. 62, no. 4, pp. 2236–2245, Apr. 2015.

[11] M. Stevic, S. Vogel, A. Monti, and S. D'Arco, "Feasibility of geographically distributed real-time simulation of HVDC system interconnected with AC networks," in *Proc. 2015 IEEE PowerTech Eindhoven*, Eindhoven, The Netherlands, Jun. 2015, pp. 1–5.

[12] M. Stevic *et al.*, "Virtual integration of laboratories over long distance for real-time co-simulation of power systems," in *Proc. 42nd Annu. Conf. IEEE Ind. Electron. Soc.*, Florence, Italy, Oct. 2016, pp. 6717–6721.
[13] B. Lundstrom, B. Palmintier, D. Rowe, J. Ward, and T. Moore, "Trans-oceanic remote power hardware-in-the-loop: Multi-site hardware, integrated controller, and electric network co-simulation," *IET Gener. Transmiss. Distrib.*, vol. 11, no. 18, pp. 4688–4701, Jul. 2017.
[14] G. Lauss, F. Lehfuss, A. Viehweider, and T. Strasser, "Power hardware in the loop simulation with feedback current filtering for electric systems," in *Proc. 37th Annu. Conf. IEEE Ind. Electron. Soc.*, Melbourne, VIC, Australia, Nov. 2011, pp. 3725–3730.
[15] A. Viehweider, G. Lauss, and F. Felix, "Stabilization of power hardware-in-the-loop simulations of electric energy systems," *Simul. Model. Practice Theory*, vol. 19, pp. 1699–1708, Sep. 2011.
[16] M. Steurer, C. Edrington, M. Sloderbeck, W. Ren, and J. Langston, "A megawatt-scale power hardware-in-the-loop simulation setup for motor drives," *IEEE Trans. Ind. Electron.*, vol. 57, pp. 1254–1260, May 2010.
[17] A. Monti, F. Ponci, Z. Jiang, and R. Dougal, "Hardware-in-the-loop testing platform for distributed generation systems," *Int. J. Energy Technol. Policy*, vol. 5, no. 2, pp. 241–257, Jan. 2007.
[18] L. Gauchia and J. Sanz, "A per-unit hardware-in-the-loop simulation of a fuel cell/battery hybrid energy system," *IEEE Trans. Ind. Electron.*, vol. 57, pp. 1186–1194, May 2010.
[19] S. Grubic, B. Amlang, W. Schumacher, and A. Wenzel, "A high performance electronic hardware-in-the-loop drive-load simulation using a linear inverter," *IEEE Trans. Ind. Electron.*, vol. 57, pp. 1208–1216, May 2010.
[20] S. Suryanarayanan, W. Ren, M. Steurer, F. Ribeiro, and G. Heydt," "A real-time controller concept demonstration for distributed generation interconnection," in *Proc. IEEE Power Eng. Soc. Gen. Meeting*, Montreal, QC, Canada, Jun. 2006, 3 pp.
[21] P. Crolla, A. J. Roscoe, A. Dysko, and G. Burt, "Methodology for testing loss of mains detection algorithms for microgrids and distributed generation using real-time power hardware-in-the-loop based technique," in *Proc. IEEE 8th Int. Conf. Power Electron. ECCE Asia*, Jeju, South Korea, Jun. 2011, pp. 833–838.
[22] B. Lundstrom, M. Shirazi, M. Coddington, and B. Kroposki, "An advanced platform for development and evaluation of grid interconnection systems using hardware-in-the-loop: Part III–grid interconnection system evaluator," in *Proc. IEEE Green Technol. Conf.,* Denver, CO, USA, Apr. 2013, pp. 392–399.
[23] O. Mohammed, M. A. Nayeem, and A. Kaviani, "A laboratory based microgrid and distributed generation infrastructure for studying connectivity issues to operational power systems," in *Proc. IEEE Power Eng. Soc. Gen. Meeting*, Minneapolis, MN, USA, Aug. 2010, pp. 1–6.
[24] F. Guo and L. Herrera, "Comprehensive real-time simulation of the smart grid," *IEEE Trans. Ind. Appl.*, vol. 49, no. 2, pp. 899–908, Mar./Apr. 2013.
[25] F. Zhang, Y. Sun, L. Cheng, X. Li, J. Chow, and W. Zhao, "Measurement and modeling of delays in wide-area closed-loop control systems," *IEEE Trans. Power Syst.*, vol. 30, no. 3, pp. 2426–2433, Sep. 2015.
[26] T. Singaraju, A. Turan, M. Gokasan, and S. Bogosyan, "Hardware-in-the-loop simulation of PUMA 560 via internet," in *Proc. 32nd Annu. Conf. IEEE Ind. Electron.*, Paris, France, 2006, pp. 5426–5432.
[27] A. Germani, C. Manes, and P. Pepe, "A new approach to state observation of nonlinear systems with delayed output," *IEEE Trans. Autom. Control*, vol. 47, no. 2, pp. 96–101, Feb. 2002.
[28] F. Cacace, A. Germani, and C. Manes, "An exponential observer with delay-dependent gain for a class of nonlinear systems with time-varying measurement delay," in *Proc. IEEE Conf. Dec. Control*, Maui, HI, USA, Dec. 2012, pp. 2364–2369.
[29] F. Cacace, A. Germani, and C. Manes, "An observer for a class of nonlinear systems with time varying observation delay," *Syst. Control Lett.*, vol. 59, pp. 305–312, May 2010.
[30] F. Cacace, A. Germani, and C. Manes, "A chain observer for nonlinear systems with multiple time-varying measurement delays," *SIAM J. Control Optim.*, vol. 52, no. 3, pp. 1862–1885, Jun. 2014.
[31] K. Ogata, *Modern Control Engineering*. 4th ed. Upper Saddle River, NJ, USA: Prentice-Hall, 2002.
[32] Z. Gajic and M. Lelic, *Modern Control Systems Engineering*. London, U.K.: Prentice-Hall, 1996.
[33] "Simscape power systems." Mathworks, Natickm, MA, USA, 2016. [Online]. Available: https://www.mathworks.com/products/simpower.html
[34] "Hardware Overview," OPAL-RT Technologies, Montreal, QC, USA, 2016. [Online]. Available: https://www.opal-rt.com/hardware-overview/
[35] "Homepage," Somerville, MA, USA, 2018. [Online]. Available: https://www.arduino.cc

James L. Cale (SM'16) received the B.S. degree (*summa cum laude*) in electrical engineering from the University of Missouri–Rolla, Rolla, MO, USA, in 2001, the M.S. and Ph.D. degrees in electrical engineering from Purdue University, West Lafayette, IN, USA, in 2005 and 2007, respectively.

From 2007 to 2010, he was a Lead Electrical Engineer, R&D, Orbital ATK. From 2010 to 2011, he was a Member of Technical Staff with Advanced Energy. From 2011 to 2017, he was a Senior Research Engineer and Group Lead with the National Renewable Energy Laboratory. He is currently an Associate Professor with Colorado State University, Fort Collins, CO, USA. His research interests include energy conversion, power electronics, finite-inertia power systems, microgrids, and power and controller hardware-in-the-loop.

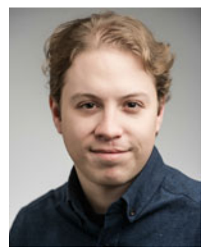

Brian B. Johnson (M'13) received the M.S. and Ph.D. degrees in electrical and computer engineering from the University of Illinois at Urbana-Champaign, Champaign, IL, USA, in 2010 and 2013, respectively.

From 2013 to 2018, he was an Electrical Engineer with the National Renewable Energy Laboratory, Golden, CO, USA. He is currently an Assistant Professor with the Department of Electrical Engineering, University of Washington in Seattle, WA, USA. His research interests include renewable energy, power electronics, and control systems.

Dr. Johnson was the recipient of National Science Foundation Graduate Research Fellowship in 2010. He is an Associate Editor for the IEEE TRANSACTIONS ON ENERGY CONVERSION.

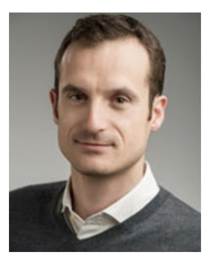

Emiliano Dall'Anese (M'11) received the Ph.D. degree in information engineering from the University of Padua, Padua, Italy, in 2011.

From 2009 to 2010, he was a Visiting Scholar with the Department of Electrical and Computer Engineering, University of Minnesota, Minneapolis, MN, USA, where he was a Postdoctoral Associate with the Department of Electrical and Computer Engineering, from January 2011 to November 2014. Since December 2014, he has been a Senior Researcher with the National Renewable Energy Laboratory, Golden, CO, USA. His research interests include advanced theory, algorithms, and analysis for optimization, control, and monitoring of large-scale cyber-physical systems.

Peter M. Young (SM'13) received the B.A. degree from Oxford University, Oxford, U.K., in 1985, the M.S. degree from the University of Florida, Gainesville, FL, USA, in 1988, and the Ph.D. degree from California Institute of Technology, Pasadena, CA, USA, in 1993, all in electrical engineering.

From 1985 to 1986, he was an Executive Engineer with British Telecom Research Laboratories, and from 1993 to 1995, he was a Postdoctoral Associate with Massachusetts Institute of Technology. He is currently a Professor with Colorado State University, Fort Collins, CO, USA. His research interests include the development of analysis and design techniques for large scale uncertain systems, and robust learning controllers, as well as a number of specific application areas. These include control of building energy management systems, optimal utilization of energy assets, and microgrids with high penetration renewable energy.

Gerald Duggan received the B.S. degree in math and computer science from New Mexico State University, Las Cruces, NM, USA, and the M.S. degree in computer science from the University of Utah, Salt Lake City, UT, USA, in 1983 and 1985, respectively.

From 1985 to 2009, he was a Senior Software Architect with Hewlett Packard, defining standards and implementing software for large-scale IT management systems. He is currently the Lab Manager of the Smart Village Microgrid Lab, Energy Institute of Colorado State University, Fort Collins, CO, USA. His research interests include village-scale microgrids, dc power distribution systems, and ac–dc efficiency studies.

Poorva A. Bedge (S'15) received the B.S. degree in electrical engineering from the Government College of Engineering Pune, Pune, India, in 2004, and the M.S. degree in electrical engineering from the University of Southern California, Los Angeles, CA, USA, in 2008. She is currently working toward the Ph.D. degree in systems engineering with Colorado State University, Fort Collins, CO, USA.

She worked in Mumbai and Delhi, India with Reliance Energy as a Senior Engineer on the electric power distribution system. At Midwest ISO, she was an Outage Coordination Engineer, and at California ISO she was a Senior Operations Planning Engineer. Her research interests include developing tools and solutions to modernize the electric grid to accommodate the rapid increase in renewable energy.

Daniel Zimmerle received the B.S. and M.S. degrees in mechanical engineering from North Dakota State University, Fargo, ND, USA, in 1983 and 1984, respectively.

From 1985 to 2005, he worked in various roles at Hewlett Packard and Agilent Technologies including both a division R&D and General Manager. From 2006 to 2007, he was the Chief Operating Officer with Spirae, Inc. He is currently a Senior Research Associate and the Director of the Electric Power System Laboratory, Energy Institute, Colorado State University, Fort Collins, CO, USA. His research interests include microgrids and the development, integration, and field assessment of distributed, renewable, and waste heat electrical generation systems.

Leah Holton received the B.S. degree in mathematics and the B.S. degree in engineering from James Madison University, Harrisonburg, VA, USA, in 2012, and the M.S. degree in mechanical engineering from Arizona State University, Tempe, AZ, USA, in 2014.

She is currently a Solar Engineer with the Independent Engineering Group, ICF, Denver, CO, USA. She supports solar energy project owners and investors with due diligence and owners engineering services.